2013

Broadband Fourier transform rotational spectroscopy for structure determination: The water heptamer

Cristóbal Pérez
University of Virginia, cp5ws@virginia.edu

Simon Lobsiger
University of Virginia

Nathan A. Seifert
University of Virginia

Daniel P. Zaleski
University of Virginia

Berhane Temelso
Bucknell University, berhane.temelso@furman.edu

See next page for additional authors

Chemical Physics Letters 571 (2013) 1–15

Contents lists available at SciVerse ScienceDirect

Chemical Physics Letters

journal homepage: www.elsevier.com/locate/cplett

Frontiers Article

Broadband Fourier transform rotational spectroscopy for structure determination: The water heptamer

Cristóbal Pérez [a], Simon Lobsiger [a], Nathan A. Seifert [a], Daniel P. Zaleski [a], Berhane Temelso [b], George C. Shields [b,*], Zbigniew Kisiel [c,*], Brooks H. Pate [a,*]

[a] Department of Chemistry, University of Virginia, McCormick Rd., Charlottesville, VA 22904-4319, USA
[b] Dean's Office, College of Arts and Sciences, and Department of Chemistry, Bucknell University, Lewisburg, PA, 17837, USA
[c] Institute of Physics, Polish Academy of Sciences, Al. Lotników 32/46, 02-668 Warszawa, Poland

ARTICLE INFO

Article history:
Available online 17 April 2013

ABSTRACT

Over the recent years chirped-pulse, Fourier-transform microwave (CP-FTMW) spectrometers have changed the scope of rotational spectroscopy. The broad frequency and large dynamic range make possible structural determinations in molecular systems of increasingly larger size from measurements of heavy atom (^{13}C, ^{15}N, ^{18}O) isotopes recorded in natural abundance in the same spectrum as that of the parent isotopic species. The design of a broadband spectrometer operating in the 2–8 GHz frequency range with further improvements in sensitivity is presented. The current CP-FTMW spectrometer performance is benchmarked in the analyses of the rotational spectrum of the water heptamer, $(H_2O)_7$, in both 2–8 GHz and 6–18 GHz frequency ranges. Two isomers of the water heptamer have been observed in a pulsed supersonic molecular expansion. High level ab initio structural searches were performed to provide plausible low-energy candidates which were directly compared with accurate structures provided from broadband rotational spectra. The full substitution structure of the most stable species has been obtained through the analysis of all possible singly-substituted isotopologues ($H_2{}^{18}O$ and HDO), and a least-squares $r_m^{(1)}$ geometry of the oxygen framework determined from 16 different isotopic species compares with the calculated O–O equilibrium distances at the 0.01 Å level.

1. Introduction

Recent advances in high-speed digital electronics have made it possible to construct a new generation of spectrometers for molecular rotational spectroscopy [1]. These spectrometers provide instantaneous broadband signal acquisition and greatly increase the sensitivity that can be achieved in either a fixed measurement time with a limited amount of sample. For rotational spectroscopy of pulsed supersonic molecular expansions at microwave frequencies (2–40 GHz), these spectrometers can acquire the rotational spectrum over bandwidths of 10 GHz or more in a single measurement cycle lasting 40 μs or less [2]. The spectrometers have no moving parts and, in particular, do not require the setting of light source or microwave cavity resonance frequencies for each measurement. The simplicity of the spectral acquisition significantly reduces the time required to acquire a high-sensitivity molecular rotational spectrum. Molecular rotational spectroscopy can provide information about the 3D molecular structure for chemical systems that cannot be easily studied by techniques such as X-ray diffraction and nuclear magnetic resonance (NMR) spectroscopy. This article illustrates the application of broadband Fourier transform microwave spectroscopy to structure determination through the challenging problem of water clusters using the water heptamer, $(H_2O)_7$, as an example.

Molecular rotational spectroscopy has played an important role in the quantitative determination of molecular structure since its development in the 1940s. The rotational kinetic energy is quantized, through the quantization of angular momentum, leading to a discrete 'line spectrum' for the rotating molecule. The molecular Hamiltonian for the simplest model, the distortable rotor which includes the effects of centrifugal distortion, is well-known and can reproduce the molecular rotational spectrum to experimental accuracy. Modifications to this Watson Hamiltonian [3] have been developed to account for nuclear quadrupole hyperfine structure and some types of large amplitude motion, such as the internal rotation of methyl groups and other symmetric tops. The ability to analyze molecular rotational spectra has been strongly influenced by the development of quantum chemistry. Current electronic structure theory calculations can provide accurate estimates of the parameters in the molecular Hamiltonian that make it possible to identify new molecules from their experimental rotational spectrum with high confidence.

* Corresponding authors.
E-mail addresses: george.shields@bucknell.edu (G.C. Shields), kisiel@ifpan.edu.pl (Z. Kisiel), brookspate@virginia.edu (B.H. Pate).

0009-2614/$ - see front matter © 2013 Elsevier B.V. All rights reserved.
http://dx.doi.org/10.1016/j.cplett.2013.04.014

Moving beyond the simple identification of molecules by comparison of measured and calculated spectroscopic parameters, the molecular structure of a molecule can be determined through the isotopic variation of the rotational constants. Kraitchman [4] provided the straightforward connection between the isotopic variation of the moments-of-inertia and the atom positions in the principal axis frame in 1953. This substitution, r_s, method, has the advantage that it gives the position of the substituted atom free from other assumptions about the molecular structure and its practical accuracy was analyzed by Costain [5]. Using this approach, an experimental structure can be built atom-by-atom, on the basis of a series of single isotopic substitutions. However, the Kraitchman method has limitations, including the difficulty of determining small coordinates in the principal axis system due to vibrational contributions incorporated in the measured ground state rotational constants. The exact physical meaning of the substitution geometry is also uncertain. The r_s structures are generally assumed to be intermediate between the effective ground state and equilibrium geometries, [6] which makes comparisons with results of quantum chemistry calculations less direct.

Other methods to determine the molecular structure from isotopic data have been developed in part to address these issues. These methods fit the observed moments-of-inertia of all available isotopic species to a molecular structure and treat the zero-point contribution to the moments of inertia at different levels. In the most successful of such approaches Watson et al. [7] have discussed the general functional form of the mass-dependent deviation between the equilibrium and zero-point moments-of-inertia and have suggested several models, denoted $r_m^{(1)}$, $r_m^{(1L)}$, $r_m^{(2)}$ and $r_m^{(2L)}$, that satisfactorily account for the isotopic variation of vibrational contributions by means of various adjustable parameters. These models are designed to recover equilibrium-quality structures from ground state experimental data and have been successfully benchmarked for small molecules [6] and several weakly bound intermolecular complexes [8]. In practice, structure fitting using the simplest $r_m^{(1)}$ model delivers heavy atom results similar to those from the substitution method, although it is now possible to compare these directly with computed equilibrium geometries. The mass-dependent structures may still show distortions caused by small atomic principal coordinates, and accounting for large isotopic effects on deuterium substitution is often not very satisfactory. The latter often requires the $r_m^{(1L)}$ model, which accounts for such effects by introducing individual adjustable parameters for each deuterated bond. When there is an abundance of isotopic data, then these models, or the $r_m^{(2)}$ or $r_m^{(2L)}$ models might be expected to correct the problems with small coordinates and give structures that closely approximate the equilibrium structure.

In principle, any rotationally-resolved spectroscopy method that provides accurate determination of the principal moments of inertia can be used for structure determination. Molecular electronic spectroscopy, using either high-resolution frequency domain spectroscopy [9] or high time resolution rotational coherence spectroscopy, [10] has been an important technique for structural studies of large molecules because of the high sensitivity of ultraviolet (UV) spectroscopy. Molecular rotation–vibration spectroscopy can also be used to determine the rotational constants, however, these spectra are often perturbed by vibrational interactions that complicate the spectroscopic analysis. The vibrational spectra of the hydride stretches, for example, are often extensively perturbed by weak interactions with the high local density of vibrational states and these spectra often provide more information about the intramolecular vibrational energy redistribution (IVR) dynamics than the molecular structure [11]. Rotationally resolved spectroscopy of the lowest vibrational modes, often associated with large amplitude motion and tunneling, can yield spectra that contain both high quality information about the molecular structure and the large amplitude vibrational dynamics. However, these spectra are challenging to acquire at high sensitivity due to the limitations of high-resolution frequency-domain instruments in the Terahertz (THz) spectroscopy region and the fact that these vibrational bands can have weak intensity. It should also be borne in mind that isotopic changes in moments of inertia become proportionally smaller with the size of the molecule, so that precise experimental determination of rotational constant values (usually better than 0.001 MHz) is required and is not yet possible with most of the above-mentioned methods.

Molecular rotational spectroscopy has proved to be the most powerful method for obtaining rotationally-resolved spectra. The technique has wide applicability with the only formal requirement being that the molecule is polar (although even non-polar molecules can have weak pure rotational spectra allowed through centrifugal distortion). A significant advance in instrumentation for molecular spectroscopy was the introduction of cavity-enhanced Fourier transform microwave spectroscopy of pulsed jets by Balle et al. [12] in 1979. The Balle–Flygare cavity design used the intrinsic time-resolution of Fourier transform microwave spectroscopy to measure the pure rotational spectrum of molecules cooled in seeded molecular beams. The important advantages of pulsed jet samples first recognized in electronic spectroscopy, the dramatic reduction in the rotational temperature and significant vibrational cooling, increased the measurement sensitivity and simplified the molecular rotational spectrum. In addition, pulsed jet sources made it possible to study new types of molecular systems including weakly bound complexes and clusters formed in the pulsed jet expansion. The development of pulsed jet sources that can produce novel chemical species is still an active field of research and pulsed electric discharge [13–16] and laser ablation [17,18] sources are now commonly used in molecular rotational spectroscopy.

The determination of molecular structure from rotational spectroscopy in pulsed molecular beams remains an essential tool for chemistry and has unique capabilities for the study of conformationally flexible molecules [18] and molecular clusters [19]. Both of these problems deal with the role of intermolecular forces in determining the complex potential energy landscapes of flexible molecular systems. In general, the standard tools of structural chemistry, X-ray diffraction and NMR spectroscopy, cannot be applied to these systems. These problems also present a common set of experimental challenges. For example, the sample being studied typically contains a larger number of distinct molecular species (many conformers of a flexible molecule, isomers of complexes of two larger molecules, and several low energy minima of clusters formed from several smaller molecules, like water). The high spectral resolution of rotational spectroscopy and spectral simplification associated with rotational and vibrational cooling in pulsed molecular beams makes it possible to analyze these mixtures with little impact from spectral congestion of overlapping spectra. For larger molecular systems, the changes in the moments of inertia (or rotational constants) can be small for different conformers or cluster geometries. The availability of accurate molecular Hamiltonian models for the pure rotational spectrum makes it possible to 'fit' the spectrum to experimental accuracy in most cases and to determine the moments-of-inertia to high accuracy in the absence of effects from vibrational interactions that can lead to effective rotational constants that include non-resonant perturbations.

The promise of molecular rotational spectroscopy is the generation of accurate three dimensional structures through the observation and analysis of spectra of many isotopologues in natural abundance. In practice, this usually means determining the heavy atom structure (where heavy atoms are defined as non-hydrogen atoms) through the isotopologues measured in natural abundance. For example, the natural abundances of ^{13}C, ^{15}N, and ^{18}O are about

1.1%, 0.36%, and 0.21%, respectively and a measurement of the normal species with about 1500:1 signal-to-noise ratio makes it possible to analyze the isotopic species incorporating a single substitution of these elements. The low natural abundance of deuterium (0.012%) makes it challenging to determine the hydrogen atom positions by rotational spectroscopy at natural abundance. The goal of producing an actual molecular structure is somewhat unique in spectroscopic studies of larger molecules and molecular clusters. The vast majority of spectroscopy studies, including most rotational spectroscopy measurements, identify the molecular geometry by a comparison of the experimental spectroscopic parameters (rotational constants in rotationally-resolved measurements and vibrational frequencies for vibrational studies) with results from computational chemistry. Although these studies can provide strong confirmation of the presence of a structure, they often fall short of actually providing tests of the accuracy of quantum chemistry calculations.

There are significant challenges to developing molecular rotational spectroscopy instruments that can routinely provide molecular structures of interest in chemistry. In many cases, such as studies of molecular clusters, there is not a complete and reliable set of theoretical structures available at the outset of the experiment to guide the experimental measurement. As a result, instruments that provide unbiased measurements by acquiring the spectrum over a wide spectral bandwidth are advantageous. High measurement sensitivity and spectral resolution are needed to obtain the spectrum of the 'normal species' as well as of a possibly large number of isotopically substituted isomers (using natural isotopic abundances or 'isotope spiking' in some cases). Finally, the spectrometer needs to operate at low frequency to match the peak spectral intensity of jet-cooled large molecules and clusters. The design of low frequency microwave spectrometers (typically operating from 2 to 8 GHz) is a special challenge given the long wavelengths involved and, for example, may necessitate the use of large mirrors if cavity-enhanced FTMW spectroscopy is used [20].

Over the past few years we have proposed and optimized the design of a new type of a microwave Fourier transform spectrometer featuring chirped-pulse excitation (CP-FTMW) for applications to the structure determination of conformationally rich molecules and molecular clusters. The present capabilities of CP-FTMW spectrometers operating in the 2–8 GHz and 6–18 GHz frequency ranges are illustrated by the structure determination of the water heptamer reported herein. This work combines theoretical techniques to identify candidate water cluster geometries, high level quantum chemistry calculations to obtain equilibrium geometries and energies for these cluster structures, and broadband rotational spectroscopy to provide quantitative structures that directly test the accuracy of the theoretical structures.

1.1. Structural features of water clusters

The goal for broadband rotational spectroscopy studies of water clusters is to experimentally determine the cluster structure without relying on electronic structure theory. There are three different aspects of water cluster structure that are considered in the study of the water heptamer: (1) The oxygen-atom framework geometry, (2) the hydrogen bond network geometry, and (3) the conformational structure of the 'dangling' O–H bonds. The framework geometry describes the basic structure of the water cluster and plays the dominant role in determining the moments-of-inertia (and, therefore, the rotational constants) of the cluster. For a given framework, there can be many different orientations of the water molecules to create the structure's hydrogen bond network. Because this structural feature involves the relative positions of the lighter hydrogen atoms, it has a relatively small effect on the moments of inertia of the full cluster. However, the network geometry causes distinct distortions in the framework geometry and, as a result, a precise experimental framework geometry is important for determining the hydrogen bond network geometry. The network geometry influences the cluster dipole moment so that spectral intensity patterns can also be used to support the determination of the network geometry. The conformations of the free O–H bonds are most difficult to determine from rotational spectroscopy.

Finally, there is another level of water cluster structure that we do not consider for the water heptamer – the permutation of hydrogen atom positions from tunneling. Each water cluster geometry (framework and network) can have several identical minima on the full potential energy surface that interchange the positions of the nuclei. This is most important for hydrogen atoms that may tunnel between these minima. For the ring structure of the water trimer [21] and pentamer, [22] tunneling from 'flipping' the free O–H position has been examined previously. The water hexamer cage shows an interesting tunneling effect called 'bifurcation tunneling' where hydrogen atom exchange in a double-donor water can occur through a rotation about the water molecule's own C_2-axis [23,24]. These tunneling dynamics are of primary importance for Terahertz spectroscopy studies which can directly excite the tunneling motion. However, tunneling effects have also been observed in the water hexamer prism and decamer by broadband rotational spectroscopy [19]. The pure rotational spectra of the two water heptamers observed in the present work show no signs of tunneling.

1.2. Theoretical chemistry techniques to identify water cluster isomers

For a given water cluster $(H_2O)_n$, the number of hydrogen bonded topologies, g_n increases exponentially with the number of waters, n. While these topologies may be generated manually for small clusters ($n < 6$), [25] a more systematic and automated approach is necessary for larger clusters due to the vast number of cluster configurations. For example, the number of unique water heptamer (g_7) and decamer (g_{10}) topologies is in the hundreds and thousands range, respectively [26]. Tools like Monte Carlo [27,28], molecular dynamics [29], genetic algorithms, [30,31] and others [32,33] have been used to search for water cluster configurations. In our case, we employed molecular dynamics (MD) configurational sampling with the TIP4P [34] water model as implemented in AMBER9 [35] to locate a large number of configurations and applied ab initio quantum mechanical (QM) methods on the low energy configurations [36,37]. In these two-step gas phase MD simulations, the $(H_2O)_7$ system was first heated from 5 K to 250 K over a period of 1 ns, then allowed to remain at 250 K for a 9 ns run. We took 200 snapshots from this 10 ns simulation at evenly spaced intervals and used them as starting structures for more reliable geometry optimizations employing second-order Møller–Plesset perturbation theory (MP2) [38].

MP2, and particularly in its more efficient resolution-of-the-identity MP2 (RI-MP2) implementation, [39] has been shown to be accurate in modeling water clusters by a large number of benchmarking studies [36,37,40–44]. MP2 is the cheapest ab initio method that is able to describe non-covalently bound systems because it includes electron correlation. When applied with correlation consistent basis sets (aug-cc-pVNZ = aVNZ), [45,46] it captures hydrogen bonding very well. We optimized the low energy structures using RI-MP2 method and aug-cc-pVDZ (aVDZ) basis set. Also, the harmonic vibrational frequencies needed to calculate the zero-point vibrational energy (ZPVE) and finite temperature thermodynamic corrections to the enthalpy (H) and entropy (S) were determined using the RI-MP2/aVDZ basis set. The RI-MP2 complete basis set (CBS) limit energies were calculated using an inverse 4–5 polynomial basis set extrapolation scheme that has been used extensively for water clusters [36,37,47,48] The RI-MP2/CBS

electronic energy (E_e) was combined with the ZPVE and finite temperature thermodynamic corrections to get the Gibbs free energy, G(T) assuming ideal gas conditions with a rigid-rotor approximation for molecular rotations and a harmonic oscillator model for vibrations.

1.3. Chirped pulse Fourier transform microwave spectroscopy

Chirped-pulse Fourier transform microwave spectrometers acquire the molecular rotational spectrum over a broad frequency range in each measurement. The first CP-FTMW spectrometer was developed for operation in the 7–18 GHz frequency range [2]. Advances in high-speed digital electronics have greatly simplified the experimental set up of CP-FTMW spectrometers, especially for low frequency operation. We have recently completed the construction of a CP-FTMW spectrometer that can be rapidly converted between 2–8 GHz and 6–18 GHz frequency operation. The component upgrades to the 6–18 GHz spectrometer include the incorporation of a 300 W peak power pulsed traveling wave tube amplifier (Applied Systems Engineering 167X/KU) that uses the WRD-650 specification of double-ridge waveguide on its output. This change, coupled with a new microwave horn antenna set using this waveguide (ATM-650-442-C1), provides low frequency coverage down to about 6 GHz – about 1 GHz lower than our previous design. The chirped pulse is generated using an 8-bit, 24 Gs/s arbitrary waveform generator (Tektronix AWG 7122B with channel interleave) and the enhanced frequency bandwidth of the spectrometer exceeds the practical output bandwidth of the AWG. A pulse generation circuit has been designed that uses frequency multipliers to extend the bandwidth of the AWG for chirped pulse creation. This circuit uses an input frequency range of 2–8 GHz from the AWG and generates microwave output in the 6–18 GHz range.

A schematic of the 2–8 GHz CP-FTMW spectrometer is shown in Figure 1 and is based on a design we presented previously [49]. The selection of new components in this spectrometer has greatly improved performance. The gas sample is excited by a microwave pulse with a linear frequency sweep (chirp) from 2 to 8 GHz and 4 μs duration. In this case, the chirped pulse is directly generated by the 24 Gs/s AWG and input to the microwave power amplifier. The pulse is amplified to about 600 W peak power using a traveling wave tube amplifier (Applied Systems Engineering 167S/C). The amplified chirped pulse is coupled to the spectrometer using a microwave cable. Inside the vacuum chamber of the spectrometer, the excitation pulse is broadcast using a high gain (high directionality) microwave horn antenna (Q-Par Angus WBH 2-18-NHG). A second horn antenna is used for the receiver and is placed 140 cm from the broadcast horn. There is space for 5 pulsed molecular beam sources in between the broadcast and receive horn antennas. Outside the chamber there is a high power PIN diode limiter (Advanced Control Components) followed by a PIN diode switch (ATM Microwave) with 20 ns rise and fall times that protects the low-noise amplifier from the amplified excitation pulse. Following excitation of the sample from the pulsed jet molecular beam sources, the coherent molecular emission, or free induction decay, is amplified and then digitized using an 8-bit, 25 Gs/s digital oscilloscope (Tektronix DPO 73304D). The digitizer is triggered using a marker channel from the AWG so that synchronous pulse-to-pulse operation is achieved permitting time domain signal averaging. Sensitivity is increased by performing averages of the FID in the time domain and the rotational spectrum is produced by fast Fourier transformation of the averaged coherent emission.

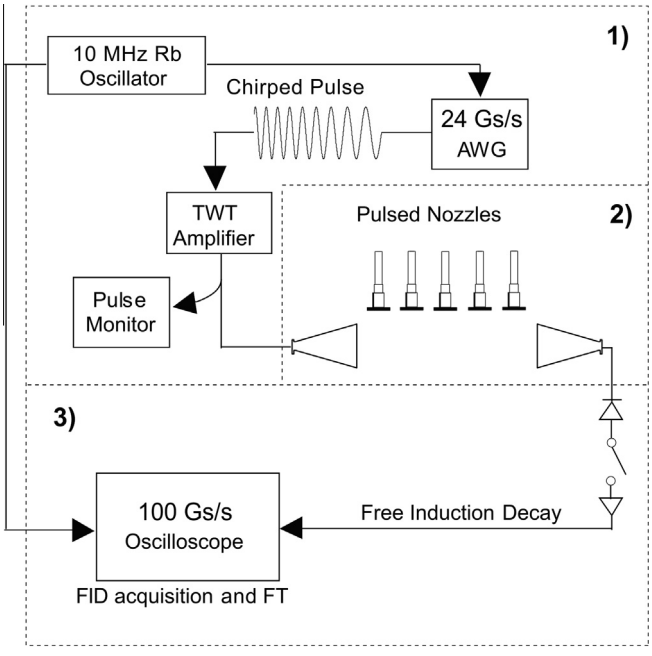

Figure 1. Schematic of the 2–8 GHz CP-FTMW spectrometer. The schematic is divided into three parts: (1) Pulse generation and amplification; (2) High vacuum chamber and sample injection; (3) FID amplification and detection.

Several instrument upgrades have increased the sensitivity of the current spectrometer by about an order-of-magnitude over the previous design. Most important, the current set of horn antennas has higher directionality with significantly improved performance below about 3 GHz. With these horn antennas it has been possible to lengthen the distance between the broadcast and receive antennas to accommodate additional pulsed molecular beam sources. As has been discussed before, the ability to use multiple molecular beam sources to increase the number of molecules in the spectrometer is important for CP-FTMW spectrometer [2]. The use of N pulsed molecular beam sources reduces the measurement time required to reach a target sensitivity by N^2 and reduces the sample consumption by a factor of N relative a spectrometer with a single molecular beam source. The high-power microwave amplifier uses a traveling wave tube with low noise power (100 mW broadband noise power) and this has also improved the spectrometer performance and makes it possible to perform double-resonance measurement directly with programmed arbitrary waveforms.

Multiple measurements are performed on each pulse sample injection cycle to decrease the measurement time and sample consumption. For each injection of gas into the spectrometer, the AWG waveform has 10 back-to-back chirped excitation pulses separated by 45 μs. The marker channel triggers the digitizer for each of these 10 pulses and the digitizer acquires a 40 μs data trace (1 million points). These 10 FID acquisitions are first co-added and then the 10 average FID record is transferred to standard memory for subsequent time-domain averaging. This 'fast frame' measurement mode has been optimized by Tektronix for signal throughput and the spectrometer can operate at 7.5 Hz repetition rate for the gas sample injection (75 Hz for FID collection or 270 K FID averages in 1 h). This is a factor of 9 improvement in the data collection rate over the previous spectrometer. This direct digital design has exceptional phase stability and it is now feasible, and routine, to acquire 10 M time-domain averages of the FID. For typical gas sample conditions (0.1% of the molecule being studied diluted in neon), each nozzle injects about 10 nmol per pulse for a total sample consumption of 50 mmol for a 10 M average spectrum.

The gas sample in the water cluster study was prepared by passing neon over a room-temperature liquid reservoir containing

water that was located outside the spectrometer. The neon pressure was 4 atm (giving a richer sample concentration of about 1% to promote the formation of larger clusters) and was selected to optimize the signals for the cage isomer of the water hexamer. The higher carrier gas pressure used in the water cluster work places a high load on the vacuum chamber pumps and the repetition rate of the pulsed valves needed to be reduced to 3.3 Hz (118 K FID averages per hour) to give optimum cluster signals. Rotational spectra in the 2–8 GHz frequency region were acquired for a pure water sample and a sample that was a 1:9 mixture of $H_2{}^{18}O$:$H_2{}^{16}O$. The analysis of the water heptamer structure also uses spectra in the 6–18 GHz spectral region that use pure $H_2{}^{18}O$, a 1:3 mixture of $H_2{}^{16}O$:$H_2{}^{18}O$, and a 1:8 mixture of D_2O:$H_2{}^{16}O$. The lists of assigned rotational transitions and the spectroscopy analysis results for all analyzed water heptamer isotopic species are available in the supplemental material.

1.4. Data analysis

Analysis of a broadband spectrum consisting of interspersed sets of transitions originating from many different carrier species poses considerable challenges, which are stimulating the development of suitable tools. The crucial first step is fishing out a consistent set of lines belonging to a given species. In fact most, though not all, of the water cluster species identified so far in the chirped-pulse spectrum have been assigned with the powerful program AUTOFIT developed in the Virginia laboratory [50]. This code utilizes the brute-force assignment method by inspecting suitably filtered combinations of three measured transitions from the actual spectrum. Once suitable candidate combinations of rotational constants were identified, the data set and its fit was expanded with the program JB95, [51] and then further refined with the AABS package for *Assignment and Analysis of Broadband Spectra*, [52,53] relying on the SPFIT/SPCAT program package [54,55] for constructing a wide range of candidate Hamiltonians. Least-squares structural fits were carried out with program STRFIT [8] and substitution coordinates were evaluated with program KRA, both available on the PROSPE website [56,57]. Molecular graphics were performed with the UCSF Chimera package [58]. Chimera is developed by the Resource for Biocomputing, Visualization, and Informatics at the University of California, San Francisco (supported by NIGMS P41-GM103311).

1.5. Broadband rotational spectroscopy measurements

The spectrum, which is presently established to be due to the water heptamer species with the strongest spectrum, was observed in the previous study of the water hexamer isomers [19] where it was assigned to a prism structure based on comparison of the experimental and the theoretical rotational constants. The cluster size distribution in the pulsed supersonic expansion can have a wide spread. The smaller clusters will have the maximum in their rotational absorption profile at a relatively high frequency. The heptamer spectrum peaks in intensity at about 8 GHz and, therefore, can be observed with good sensitivity in either the 6–18 GHz or the 2–8 GHz spectrometer. We have analyzed the rotational spectra of isotopologues of the previously identified water heptamer using spectra acquired with the two different configurations. Altogether 30 different isotopic clusters that have been assigned: $(H_2{}^{16}O)_7$ (spectra in 2–8 GHz and 6–18 GHz regions), $(H_2{}^{18}O)(H_2{}^{16}O)_6$ (spectra in 2–8 GHz and 6–18 GHz), $(H_2{}^{18}O)_7$ (spectrum in 6–18 GHz), $(H_2{}^{16}O)$ $(H_2{}^{18}O)_6$ (spectra in 6–18 GHz), and $(HOD)(H_2{}^{16}O)_6$ (spectra in 6–18 GHz).

The 'isotopic satellites' in the rotational spectra of the $H_2{}^{18}O$ (2–8 GHz spectrum) and HOD (6–18 GHz spectrum) substituted clusters are shown in Figure 2. For the $(H_2{}^{18}O)$ $(H_2O)_6$ isomers, the spectra all have approximately equal spectral intensity reflecting the statistical incorporation of the isotopically labeled water. However, in the $(H_2O)_6$(HOD) isotopologues the 4 spectra where the –OD does not participate in a hydrogen bond are about 2 times weaker than the spectra where the –OD bond participates in the cluster's hydrogen bond network. The energetic preference for

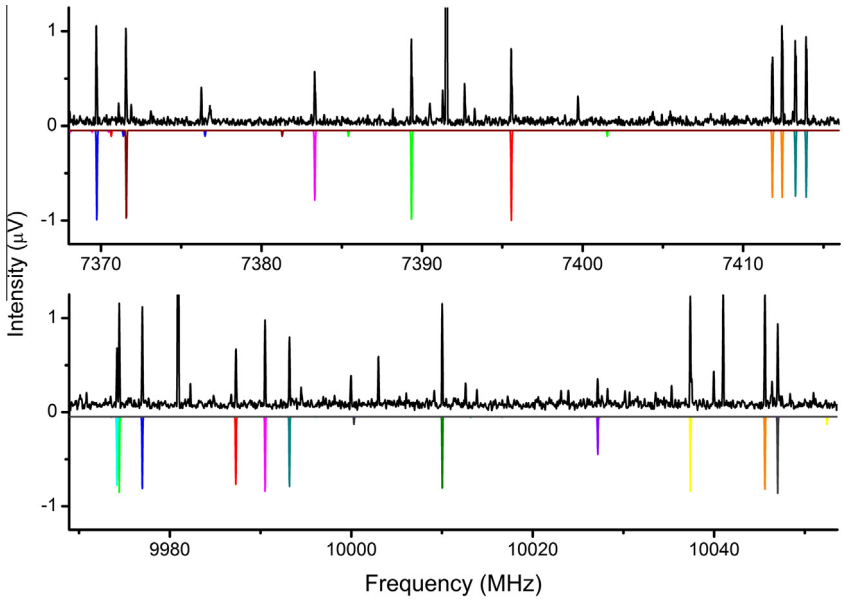

Figure 2. The top panel shows a segment of the experimental CP-FTMW spectrum of water in the 2–8 GHz frequency region. The black trace is the experimental spectrum, and the colored traces are 1.5 K (rotational temperature) simulations of the observed seven single $(H_2{}^{18}O)$ $(H_2O)_6$ species of the stronger water heptamer. The final spectrum was obtained after a total of 11 000 000 FIDs were coadded in the time domain resulting by flowing neon over an $H_2{}^{18}O$:$H_2{}^{16}O$ sample enriched to a 1:9 ratio. The bottom panel shows a segment of the water spectrum in the 6–18 GHz frequency range. The black trace is the experimental spectrum and the colored traces represent 1.5 K simulations of several single $(H_2O)_6$(HOD) isotopologues of the stronger water heptamer. The final spectrum is the result of coadding 8 700 000 FIDs in the time domain. A 1:8 mixture of D_2O:$H_2{}^{16}O$ was used to preferentially incorporate a single HDO molecule in the structure of the cluster. The violet trace shows a simulation of one of the spectra where the –OD does not participate in a hydrogen bond. The intensity is seen to be reduced by a factor of ~2. See text for further explanation.

Table 1
Spectroscopic constants for the two observed isomers of the water heptamer.

	HEPT1	HEPT2
A (MHz)[a]	1304.43555(72)[b]	1345.15942(80)
B (MHz)	937.88441(61)	976.8789(10)
C (MHz)	919.52364(57)	854.47389(89)
Δ_J (kHz)	0.4567(41)	0.439(13)
Δ_{JK} (kHz)	−0.342(21)	[0]
Δ_K (kHz)	0.842(25)	[0]
δ_J (kHz)	0.0377(29)	0.0497(98)
δ_K (kHz)	0.63(21)	[0]
N[c]	59	30
σ (kHz)[d]	6.21	7.18
μ_{rel} (a:b:c)[e]	1: 1: –	1: –: 1

[a] A, B, and C are rotational constants and Δ_J, Δ_{JK}, Δ_K, δ_J, δ_K are quartic centrifugal distortion constants in Watson's A-reduced asymmetric rotor Hamiltonian.
[b] Errors in parentheses are standard errors in units of the last digit.
[c] The number of fitted lines.
[d] Standard deviation of the fit.
[e] Approximate relative magnitudes of μ_a, μ_b, and μ_c dipole moment components estimated from relative intensities of corresponding types of rotational transitions (unobserved transition type is denoted by –).

having an –OD hydrogen bond donor is often explained by the lower zero point vibrational energy in the large amplitude bond.

We have also identified a second, weaker water heptamer cluster spectrum. The rotational constants of the two $(H_2O)_7$ water heptamer species are given in Table 1. In both cases the spectrum can be fit to experimental accuracy using the Watson asymmetric top rotational Hamiltonian [3] (A-reduction) and including the quartic centrifugal distortion constants. The similarity in the rotational constants suggests that the carriers of these two spectra have similar cluster structures. The two spectra have different directions of the dipole moment in the principal axis system, indicated through the relative intensities of the a-type, b-type, and c-type rotational transitions.

1.6. The water heptamer oxygen atom framework geometry

The oxygen-atom framework gives the basic isomer structure of the water cluster. For the water heptamer, several low-energy cluster geometries have been identified and are summarized in Figure 3. Several of these structures can be obtained by adding a water molecule to the edge of one of the water hexamers – cage, prism, book, or cyclic. Others are new cluster geometries, like the 7-TW1 that includes a tetrahedral water cluster geometry. These isomers can be distinguished by rotational spectroscopy using the rotational constants. The rotational constants for the isomers from theoretical equilibrium structures are given in Table 2. Comparison of the theoretical results with the experimental results in Table 1 suggests that the $(H_2O)_7$ spectra identified in the pulsed jet measurement have the lowest energy 'prism' structure. However, the higher energy cage heptamer is also a possible match based on rotational constant comparisons and the possibility that we are observing this isomer is discussed below. We should also remember that we are comparing experimental ground state constants with calculated equilibrium values, which are usually larger since the equilibrium geometry is more compact (see Table 1 of Ref. [19]).

Table 2
Rotational parameters and energy differences for the low-energy geometries in Figure 3.

	7-PR1	7-CA1	7-Book1	7-TW1	7-CY1
A (MHz)	1334	1325	1340	1820	1077
B (MHz)	974	936	741	525	761
C (MHz)	954	839	530	521	487
μ_a (D)	0.7	3.1	0.3	−0.2	0.9
μ_b (D)	−0.7	0.2	−2.6	−0.1	1.8
μ_c (D)	0.4	−0.9	−1.1	1.5	0.7
$\|\|\mu\|\|$ (D)	1.1	3.2	2.8	1.5	2.2
ΔE (kcal/mol)	0	1.45	2.69	3.51	4.65
ΔE_0 (kcal/mol)	0	0.91	1.67	2.38	3.1
ΔG_{50} (kcal/mol)	0	0.87	1.47	2.12	2.87

1.7. The water heptamer hydrogen bond network geometry

Perhaps the greatest challenge for water cluster structure studies is the determination of the hydrogen bond network geometry. These further isomers are generated by the number of distinct water molecule orientations that can be adopted within a basic oxygen-atom framework. The enumeration of different water cluster topologies has been discussed previously [37] and can give rise to a large number of water cluster isomers for a given oxygen-atom

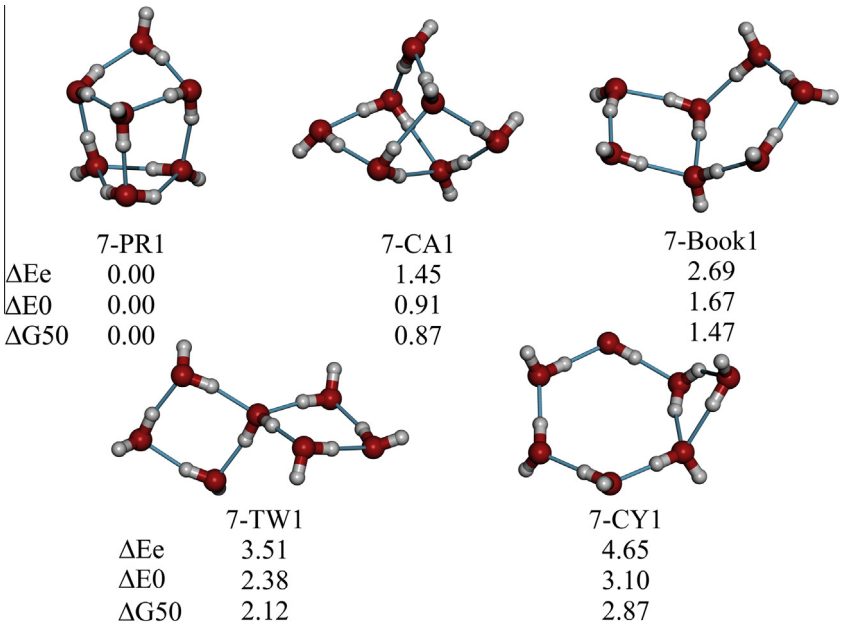

Figure 3. Several low-energy oxygen-atom frameworks of the water heptamer (energy differences in kcal/mol).

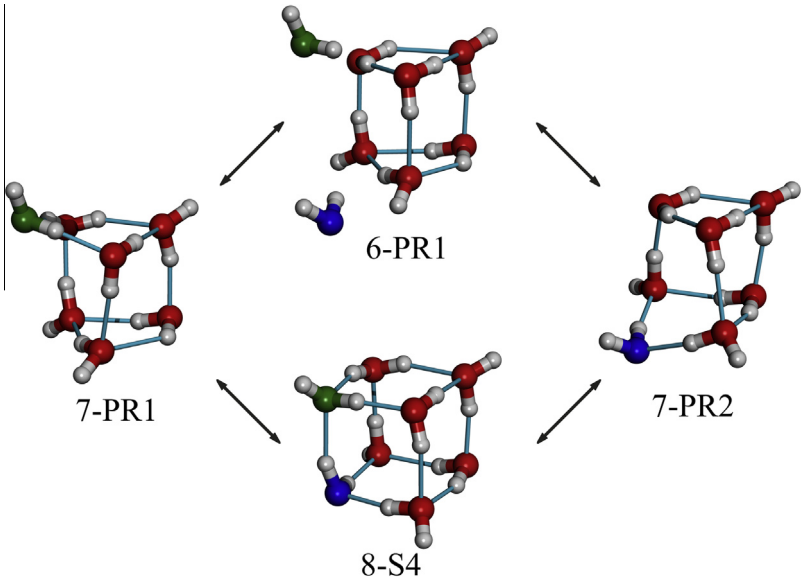

Figure 4. Generation of the two lowest-energy water heptamer isomers by adding a water molecule to the minimum energy isomer of the prism water hexamer on the top or by removing a water molecule in the water octamer on the bottom. The added or removed water molecules are highlighted in blue and green.

framework geometry, as discussed in more detail further below. The underlying reason for the large number of hydrogen bond network isomers possible for the water heptamer prism framework can be illustrated by correlating the heptamer structure with the related hexamer prism and octamer cube structures as shown in Figure 4. It can be seen how two of the low energy heptamer structures identified by theory can be derived by either adding a single water molecule to the edge of the hexamer prism or by removing a water from the water octamer. All six water molecules in the hexamer prism are distinct as shown by the observation of six isomers of the $(H_2{}^{18}O)(H_2{}^{16}O)_5$ cluster. Therefore, there are six distinct edges (three in the top and bottom 'trimer' faces) for adding a water molecule to produce a heptamer prism structure.

Furthermore, there are several different hydrogen bond network isomers of the hexamer prism with calculated energies within about 1.5 kcal/mol of the lowest energy isomer displayed in Figure 5. The four lowest energy hydrogen bond network isomers of the water prism identified in a theoretical isomer search are shown in Figure 5. Each of these hexamer prism isomers can produce heptamer prism structures by adding water to an edge. The lowest energy isomers in the heptamer prism family that have been identified by computational chemistry searches are shown in Figure 6. The first three equilibrium structures (7-PR1, 7-PR2, and 7-PR3) are related to the lowest energy hexamer prism. However, the next two isomers (7-PR4 and 7-PR5) are derived from the higher energy 6-PR2 and 6-PR3 hexamers. It is interesting to note that 6-PR2 and 6-PR3 can be viewed as stacking the experimentally known lowest energy water trimer structure with either clockwise–clockwise or clockwise–counterclockwise orientations. However, the lowest energy water hexamer prism structure, 6-PR1, does not use this trimer structure.

The rotational constants and dipole moments obtained from electronic structure theory calculations at the MP2/aVDZ level of theory are given in Table 3 for the lowest energy heptamer prism isomers that have so far been identified in isomer searches. As expected from their shared oxygen-atom framework, these isomers have similar calculated rotational constants. A direct comparison of experimental (Table 1) and theoretical rotational constants does not allow an unambiguous structure identification. The hydrogen bond network causes two key changes to the water cluster properties. The orientations of the hydrogen bonds will produce unique distortions in the oxygen-atom framework so that structural information on the oxygen atom positions can greatly aid the structure identification. Furthermore, the different water orientations in these isomers affect the cluster dipole moment in both magnitude and its direction relative to the principal axes for overall rotation.

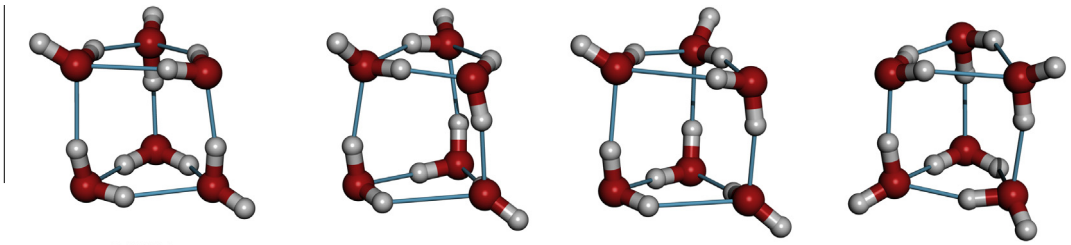

	6-PR1	6-PR2	6-PR3	6-PR4
ΔΔEe	0.00	1.20	1.23	1.58
ΔΔE0	0.16	1.20	1.31	1.41
ΔΔG50	0.18	1.19	1.32	1.41

Figure 5. The four lowest-energy hydrogen bond network isomers of the prism water hexamer.

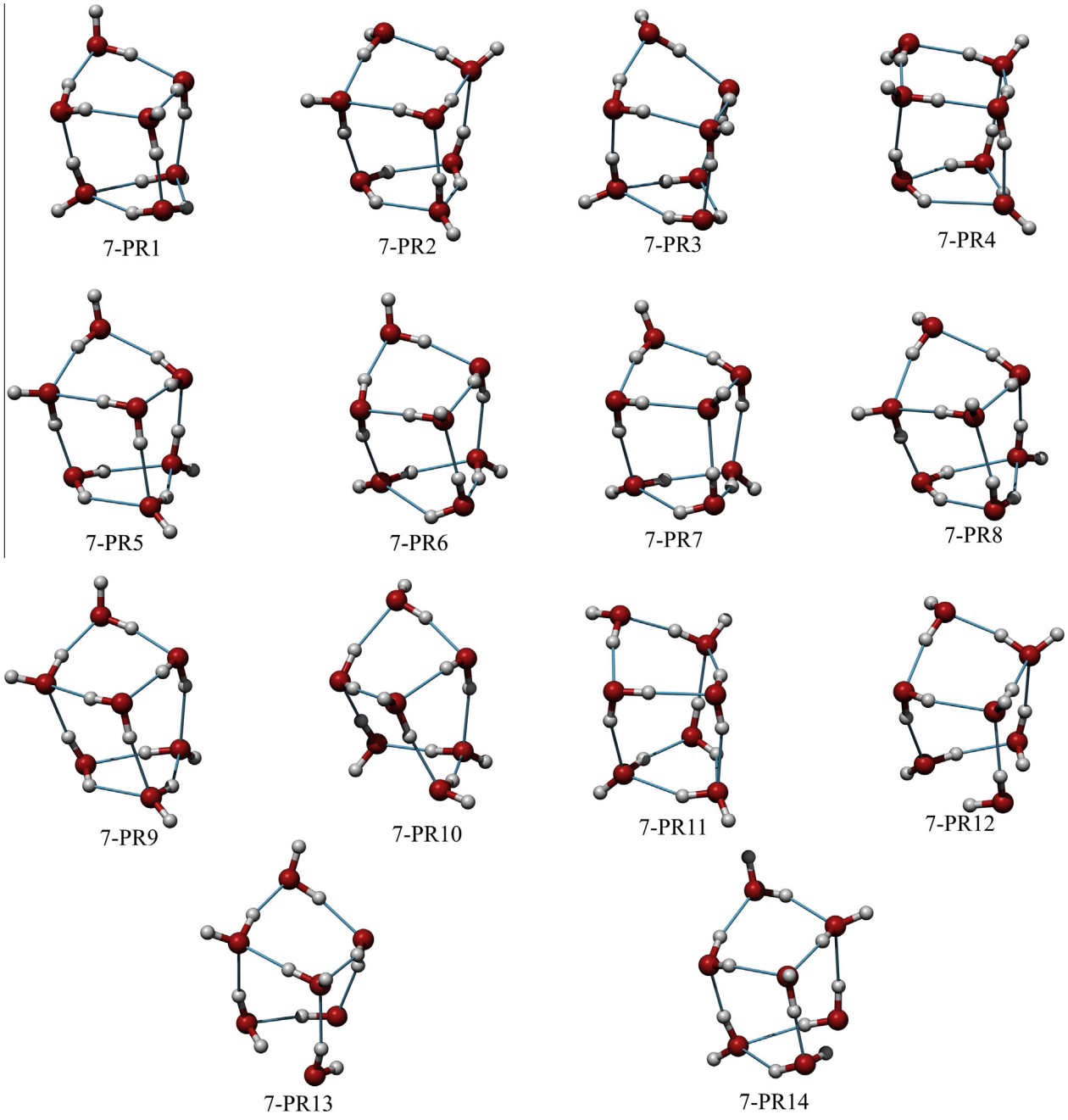

Figure 6. The lowest energy isomers in the heptamer prism family from ab initio calculations.

However, as will be discussed below, the dipole moments from equilibrium geometries of the water clusters can be misleading when large amplitude motions in the cluster are considered.

For the strongest water heptamer spectrum we have obtained the oxygen atom framework geometry from Kraitchman analysis of the $(H_2O)_7$ and seven $(H_2{}^{18}O)(H_2{}^{16}O)_6$ isotopologues and, separately, from the $(H_2{}^{18}O)_7$ and seven $(H_2{}^{16}O)(H_2{}^{18}O)_6$ isotopologues. The Kraitchman analysis returns the position of each substituted ^{18}O atom in the principal axis system individually from the differences in the moments-of-inertia to the parent (unsubstituted) molecule. However, this analysis provides only the magnitudes of the coordinates. We have chosen the signs of the coordinates to give the best correspondence to oxygen atom positions from the theoretical structures. A comparison of the experimental and theoretical oxygen atom frameworks for the two lowest energy theoretical structures (7-PR1 and 7-PR2) is shown in Figure 7. An important point about this figure is that the experimental atom positions show an overlap of two separate results – the atom positions obtained from the $(H_2{}^{16}O)_7$ parent and the $(H_2{}^{18}O)_7$ parent species. These two coordinate determinations are in excellent agreement with a root-mean-squared atom position difference of 0.04 Å.

This result provides experimental validation for using $H_2{}^{18}O$ substitution to determine the framework geometry. The experimental Kraitchman positions for each cluster are shown in Figure 7 separately on the left and also superimposed on the theoretical equilibrium geometry on the right. The selection of coordinate signs are shown in Table 4 where the distance between the experimental and theoretical oxygen atoms are also reported. The 7-PR1 and 7-PR2 are the only isomers (other than 7-PR3 discussed next) that have atom positions in general agreement with the

Table 3
Predicted rotational constants, dipole moment and energy difference for the fourteen lowest energy isomers of the PR family at MP2/aVDZ level of theory.

	PR1	PR2	PR3	PR4	PR5	PR6	PR7	PR8	PR9	PR10	PR11	PR12	PR13	PR14
A (MHz)	1334	1380	1355	1366	1407	1330	1329	1359	1439	1314	1344	1431	1372	1369
B (MHz)	974	1000	947	1012	970	958	986	977	935	937	982	934	958	968
C (MHz)	954	890	930	915	879	946	927	898	878	828	900	874	890	891
μ_a (D)	0.7	1.3	−1.5	−1.0	1.1	0.9	0.8	−2.5	1.2	3.7	2.7	−2.1	−2.5	3.5
μ_b (D)	−0.7	0.4	1.4	0.2	−1.2	0.7	0.7	−1.1	−0.9	0.2	−1.8	−1.1	−0.8	−1.7
μ_c (D)	0.4	1.0	1.9	1.3	−0.8	0.7	0.8	−0.5	−0.9	1.0	1.9	−2.6	0.6	−0.9
$\|\|\mu\|\|$ (D)	1.1	1.7	2.8	1.7	1.8	1.3	1.3	2.8	1.8	3.8	3.8	3.5	2.7	4.0
ΔE (kcal/mol)	0	0.34	0.50	0.85	0.86	1.12	1.16	1.38	1.48	1.63	1.71	1.82	1.86	1.96
ΔE_0 (kcal/mol)	0	0.42	0.25	0.92	0.71	1.03	1.12	1.26	1.36	1.14	1.55	1.62	1.7	1.78
ΔG_{50} (kcal/mol)	0	0.41	0.25	0.91	0.7	1.01	1.11	1.25	1.35	1.09	1.53	1.61	1.69	1.77

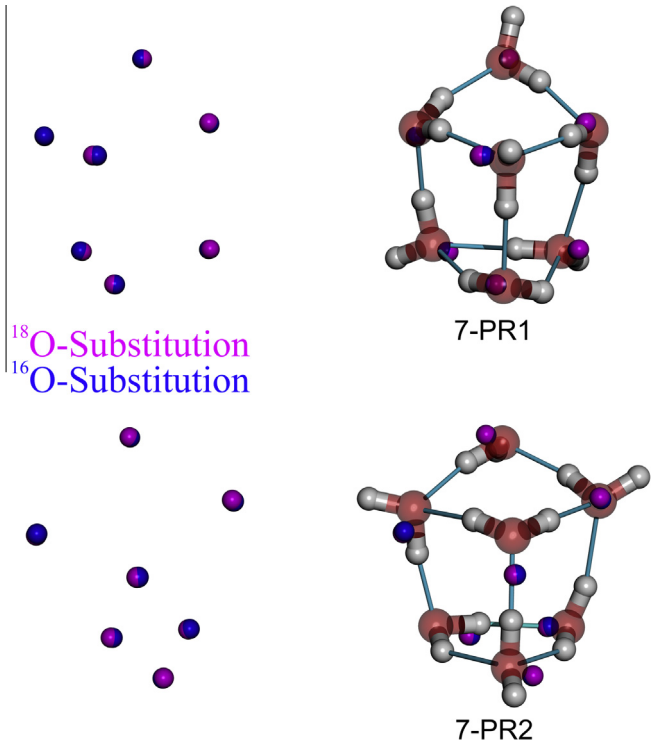

Figure 7. The two experimental Kraitchman oxygen-atom frameworks for 7-PR1 (top) and 7-PR2 (bottom) compared with the equilibrium structures using the signs in Table 4.

experimental atom positions. The agreement with 7-PR1 is better and supports the identification of the experimental cluster as the lowest energy theoretical structure, 7-PR1.

Experimental confirmation of the structure as 7-PR1 is possible using Kraitchman analysis of the $(HOD)(H_2O)_6$ spectra. Isotopic substitution of HOD is not expected to give quantitative structural information for water clusters because the deuterium substitution changes in vibration–rotation contributions to ground state rotational constants and in the resulting effects are known to be large. This is the case for both the H-atom positions in the hydrogen bond network and for the free O–H positions that can also exhibit large amplitude motion. The complete Kraitchman substitution structure for $(H_2O)_7$ is shown in Figure 8 where it is compared to the 7-PR1 equilibrium geometry from theory providing unambiguous structure determination for the dominant water heptamer species in the pulsed jet sample.

The vibrational structure of the O–H stretch fundamentals has also been shown to be sensitive to the hydrogen bond network geometry. It has been used, for example, to assign the two hydrogen bond network isomers of the cubic water octamer [59,60]. More recently, Terahertz vibration–rotation tunneling spectrum for the water octamer has also been reported [61]. A size-selected cluster study of the water heptamer O–H vibrational spectrum showed that a model for the vibrational spectrum using the 7-PR1 and 7-PR2 isomers was consistent with experiment [62]. Our experiment suggests that only one isomer dominates the pulsed jet sample, but the size-selected cluster experiments are expected to have a higher temperature. The accurate prediction of vibrational spectra of water clusters is still an active area of research and it is unclear how definitive is a hydrogen bond network assignment based on the infrared spectrum.

1.8. The conformational structure of the free O–H bonds

One structural feature of water clusters that is difficult to resolve by rotational isotopic substitution measurements is the position of the 'dangling' O–H bonds. There can be large amplitude motion that is conformational isomerization about the hydrogen bond. The two isomers identified by theory as 7-PR1 and 7-PR3 are an example of water cluster conformers that share the same

Table 4
Selection of coordinate signs and oxygen–oxygen distance comparisons between theory and the two experimental determinations.

^{16}O-coordinates			^{18}O-coordinates			PR1-signs			^{16}O-theory distances	^{18}O-theory distances	PR2-signs			^{16}O-theory distances	^{18}O-theory distances
1.078	1.976	0.732	1.083	1.951	0.788	+	–	–	0.454	0.515	+	–	+	0.594	0.544
1.070	0.310	1.799	1.074	0.288	1.801	–	–	–	0.377	0.399	–	–	+	0.805	0.804
2.489	0.639	0.327	2.487	0.652	0.312	+	+	–	0.152	0.171	–	–	–	0.997	1.005
0.214	2.094	0.798	0.211	2.122	0.723	+	+	–	0.461	0.539	+	+	+	0.748	0.769
0.930	0.898	1.608	0.932	0.865	1.626	–	+	+	0.444	0.481	–	–	–	0.430	0.396
2.908	0.532	0.255	2.908	0.542	0.242	–	–	+	0.125	0.139	+	+	–	0.411	0.396
1.117	0.778	1.776	1.122	0.815	1.757	+	–	+	0.431	0.472	–	+	–	0.857	0.898
							Average		0.349	0.388				0.692	0.687

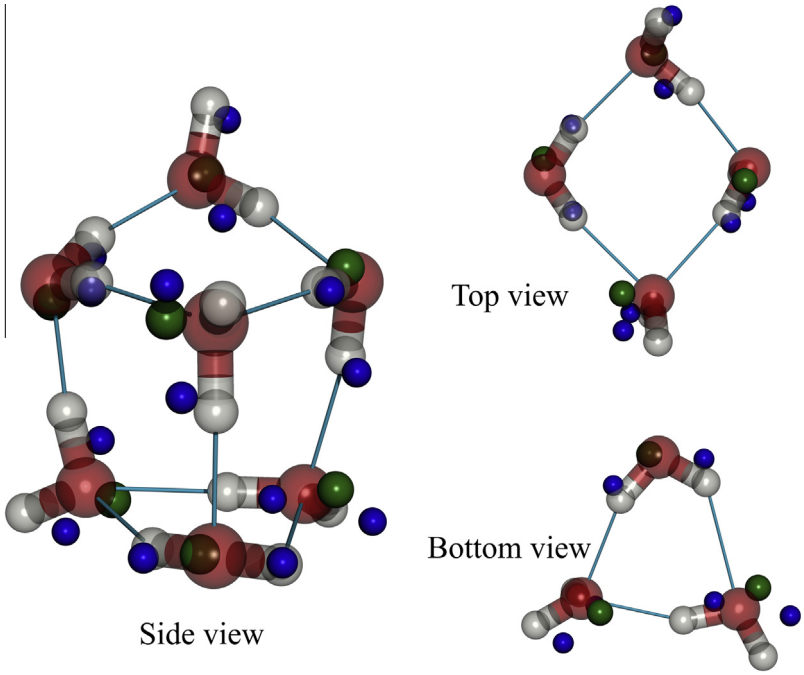

Figure 8. The complete Kraitchman substitution structure for $(H_2O)_7$ compared to the 7-PR1 equilibrium geometry at RI-MP2/aVDZ level of theory. The green spheres represent the ^{18}O coordinates while blue balls are the deuterium substitution coordinates.

framework and hydrogen bond network. A one-dimensional potential energy scan for this conformational motion is shown in Figure 9. This figure also shows how the calculated dipole moment varies as a function of the torsional angle. The barrier of the isomerization potential is on the order of the expected zero-point torsional energy so the ground torsional state is likely to be delocalized over the broad range of angles in the potential. One aspect of the delocalized free O–H bond position is that it may lead to significant differences between experimental dipole moment components and those predicted from minimum energy geometries due to averaging over the torsional probability distribution. Structure identifications that rely heavily on dipole moment information may need to consider the conformational averaging [63]. The structural delocalization of the free O–H bonds has been described before for the conformational potential energy surface of the water hexamer cage where both apical water molecules have free O–H bonds [23,64]. Even if two torsional wavefunctions with localization in the 7-PR1 and 7-PR3 wells exist, it is likely that the population would cool to the lowest energy torsional level in the pulsed jet. Therefore, we do not expect that 7-PR3 is detectable in the experiment, or probably even distinguishable from 7-PR1.

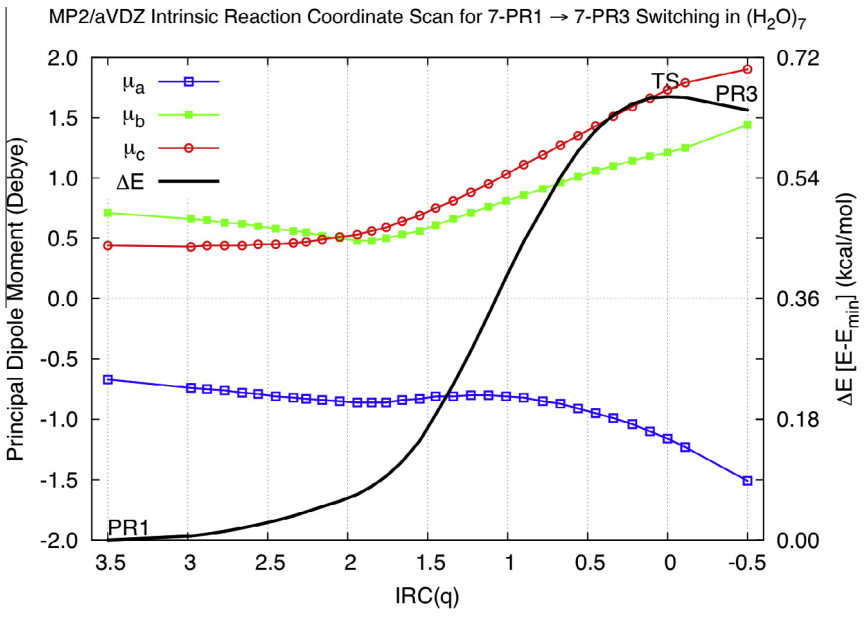

Figure 9. The change in energy (black) and principal dipole moment components (blue, green, red) along the PR1 → PR3 intrinsic reaction coordinate (q) calculated using MP2/aVDZ. 'q' is basically the dihedral angle the top free OH of the DA (single donor–single acceptor) water makes with the tetramer. It ranges from 99.7° (PR1) to 174.5° (PR3).

1.9. The experimental structure of the water heptamer

The HOD substitution experiments confirm that the hydrogen bond network of the observed cluster has the 7-PR1 geometry. The $H_2{}^{18}O$ substitution measurements can now be used to determine a quantitative experimental structure for the oxygen atom framework in a more precise structure determination that combines experiment and theory. The experimental moments-of-inertia available from oxygen substitution in the form of 16 different $H_2{}^{16}O$–$H_2{}^{18}O$ isotopic species provide abundant data for determination of the least-squares molecular structure using the $r_m^{(1)}$ method [7,8]. The primary parameters of fit are the complete set of 15 structural internal coordinates defining the seven atom oxygen framework: O–O distances, associated angles, and dihedral angles. These are augmented by three parameters of the $r_m^{(1)}$ model: c_a, c_b, and c_c. There are thus 18 adjustable parameters that are fitted to 48 experimental observables. The internal parameters of the seven complexed water molecules, r(OH) and ∠⟨HOH), are fixed at the calculated 7-PR1, RI-MP2/aug-cc-pVDZ values. The angular orientations of the water units are declared in such a way as to preserve the hydrogen bond angles ∠⟨OH···O). In fact the decisions concerning the water monomers turn out not to be critical and do not have a significant effect on the final fit. It is also possible to fit the effective ground state, r_0, geometry in a similar least-squares manner by omitting the three c parameters, although the deviation of fit turns out to be significantly poorer.

The final water heptamer structure is shown in Figures 10 and 11, while the associated Cartesian coordinates are listed in Table 5. Figure 10 compares the $r_m^{(1)}$ geometry with the substitution and theoretical structures, while Figure 11 compares the experimental and theoretical O–O distances. The agreement in the O–O distances in Figure 11 is excellent, and is at an average 0.014 Å level. This small difference is also partly due to the fact that the experimental values are on average longer than the computed ones by this amount. The level of agreement between experiment and theory is very satisfying and similar to that obtained previously for the three water hexamer species, [19] in a testimonial to the considerable advances made in determining detailed information on water clusters. The RI-MP2/aug-cc-pVDZ computation, while reliable, is an incomplete description of the one-electron basis set and n-electron correlation, while $r_m^{(1)}$ is only an approximation to the real equilibrium geometry, but this combination is proving to be very useful for benchmarking the water cluster results. Consideration of the actual O–O values reveals several interesting features of the heptamer cluster. The longest O–O distance, d(O1–O3) = 2.987(3) Å, is located in the trimer ring, Figure 11 right, and is very similar to the analogous distance in the identical top ring of the prism water hexamer (Figure 4, Ref. [19]). The associated hydrogen bond, O3–H···O1 in the heptamer, is calculated in both clusters to have the greatest deviation from linearity. It appears to be the place where the trimer ring distorts in order to compensate for the three pillar-type inter-ring hydrogen bonds, both in the heptamer and in the hexamer prism cluster. The shortest O–O distance, d(O5–O7) = 2.642(3) Å is, in fact, in the interconnecting pillar directly opposite the longest distance, and a similar situation is the case in the prism hexamer. The remaining eight O–O heptamer distances group into two relatively compact regions of values, as pointed out in Figure 11. More detailed understanding of underlying hydrogen bonding responsible for these values is possible in terms of a detailed energy decomposition for each hydrogen bond and detachment energies of individual water units from the cluster but, for reasons of brevity, this will be the subject of a separate report.

The comparison of the various complete 3D-frameworks for the water heptamer as made in Figure 10 reveals an intriguing discrepancy. The $r_m^{(1)}$ and r_s (as well as the r_0) experimental Cartesian coordinates are consistent with each other at the 0.01 Å level, and complete coordinate lists are included in the supplementary information. On the other hand the theoretical RI-MP2/aug-cc-pVDZ equilibrium geometry shows clear differences in the oxygen atom positions, as shown in the left part of Figure 10 and as already identified in Table 4. This was found to be surprising in view of the excellent agreement between experimental and computed O–O distances, until it was realized that the experimental and computed geometries can be satisfactorily aligned by a simple rotational transformation about the center of mass of the heptamer cluster. Furthermore, alternative levels of computation, such as MP2/6-311G++(d,p), deliver similar oxygen networks but at considerably different equilibrium principal coordinates. In the particular case of MP2/6-311G++(d,p), which would normally be a less preferred computation level for water clusters, the agreement of calculated principal coordinates with experiment is actually very good (supplementary information). The present working conclusion is that this results from variation in the equilibrium hydrogen positions, which tend to be more susceptible to the level of computation. On the other hand, all experimental determinations are self-consistent because they are all subject to the same effective hydrogen averaging in the ground state. We have, therefore, one further indicator that careful treatment of hydrogen averaging will be crucial for understanding water cluster geometries beyond the level of the oxygen framework and, of course, the hydrogen dynamics has been the dominant feature in the studies of the smaller water clusters [65].

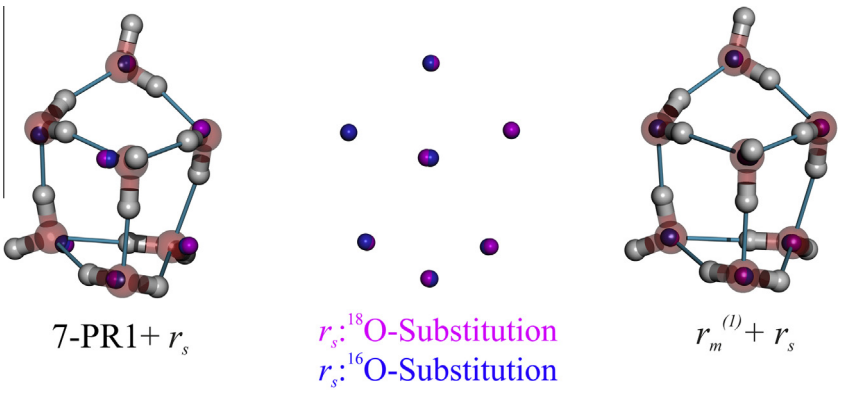

Figure 10. Comparison between the experimental oxygen frameworks obtained from two independent Kraitchman analyses (centre) and of these substitution frameworks with the calculated RI-MP2/aug-cc-pVDZ equilibrium structure (left) and the final least-squares $r_m^{(1)}$ structure (right).

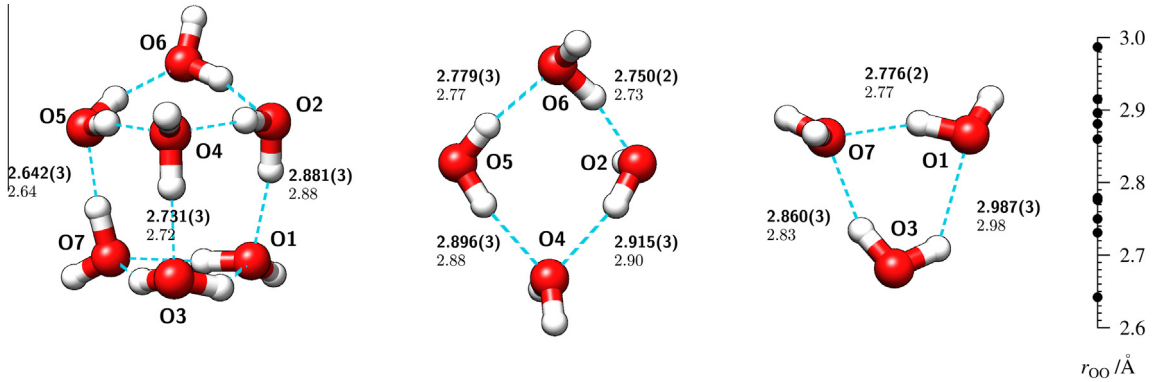

Figure 11. Comparison of experimental $r_m^{(1)}$ and the calculated O–O distances (Å) in the main water heptamer species. This structure may be viewed as a cyclic trimer and a cyclic tetramer connected by three pillars, and the two constituent rings (centre and right) are viewed from the top of the cluster depicted on the left. Each pair of numbers compares the experimental, $r_m^{(1)}$, value (upper) with the calculated RI-MP2/aug-cc-pVDZ equilibrium value (lower). Interesting banding in the O–O distances is apparent.

Table 5
$r_m^{(1)}$ principal coordinates [a,b] (Å) of the seven oxygen atoms in the water heptamer from the global fit to moments of inertia of all 16 available isotopic species.

	a	*b*	*c*
O1	1.0742(20)	−1.9412(13)	−0.7891(19)
O2	−1.0663(19)	0.2951(27)	1.7926(12)
O3	2.4752(9)	0.6511(24)	−0.2994(27)
O4	0.2064(33)	2.1061(11)	−0.7369(20)
O5	−0.9247(22)	0.8610(21)	1.6203(15)
O6	−2.8925(8)	−0.5411(28)	0.2480(20)
O7	1.1148(20)	−0.8130(22)	1.7470(14)

[a] The coordinates result from a least-squares fit of all 15 internal structural parameters necessary to describe the oxygen framework: 6 distances, 5 angles, and 4 dihedral angles, which are augmented by three $r_m^{(1)}$ parameters: c_a = 0.369(9), c_b = 0.477(8), and c_c = 0.488(8) $\mu^{1/2}$Å.

[b] The final $r_m^{(1)}$ fit to 48 moments of inertia of 16 isotopic species has a deviation of fit of 0.0162 μÅ^2 corresponding to an average obs-calc deviation in rotational constant values of 0.02 MHz.

1.10. Structural assignment of the second water heptamer

We have identified a second spectrum in the broadband rotational spectroscopy measurement with rotational constants characteristic of the water heptamer (see Table 1). However, the current spectrometer sensitivity precludes any isotopic measurements. We propose that its structure is 7-PR2, the second lowest energy isomer identified by theory. It is, however, first necessary to consider the possibility that this spectrum might arise from an excited vibrational state of 7-PR1, possibly in the 7-PR1/7-PR3 potential. The main evidence against this assignment is that the two species have different dominant dipole moment components, with the weaker spectrum being due to a species with *a*- and *c*-type transitions, while the main heptamer has *a*- and *b*-type transitions. This difference cannot be accounted for by torsional averaging. In addition, we have seen no 'satellite' spectra for the water hexamer cage, prism, and book isomers that could be attributed to excited vibrational states and the hexamer spectra have a factor of 2 higher signal-to-noise ratio than the main heptamer species.

On the basis of rotational constants alone, the second spectrum could be assigned to a different oxygen-atom framework isomer – 7-CA1 derived by adding one water to the hexamer cage. The agreement between experimental and theoretical rotational constants is about the same for 7-CA1 and 7-PR2, although for 7-CA the calculated constants are higher than from experiment (in contrast to the lower calculated values relative to experiment for 7-PR1). On the other hand the scaling factors of the rotational constants between theory and experiment for the 7-PR2 structure are nearly the same as for 7-PR1, in support of the 7-PR2 assignment. A more decisive argument against assignment to 7-CA1 is that theory predicts that the intensity of *a*-type transitions relative to *c*-type transitions would be 10:1 for 7-CA1, whereas we observe these two transition types at near equal relative intensity. The relative intensities in the observed spectrum are thus in better agreement with the theoretical predictions for 7-PR2.

2. Discussion

Broadband rotational spectroscopy has unique features that make it well suited to study molecular structure. One important aspect of the measurement is that it provides an unbiased survey spectrum of all of the molecular species in the pulsed jet gas sample. This is a significant shift in the way supersonic expansion rotational spectroscopy studies are usually performed. The narrow-band performance of cavity FTMW spectrometers encourages targeted search measurement strategies where a molecule of interest is decided on before the measurement. Its spectroscopic parameters (rotational constants and dipole moments) are estimated by theory and used to define the initial frequency search range. The collection of enough data for a full spectroscopy assignment proceeds by bootstrapping the analysis leading to even narrower target search ranges as the spectrum analysis converges. For studies like the present one on water cluster structures, there may not be a reliable list of candidate structures at the outset and the pulsed jet sample will create a wide distribution of water clusters so the spectrum can have high transition density that makes targeted search/bootstrapping approaches less efficient.

A second advantage of CP-FTMW spectroscopy is that it has a large, useable dynamic range. This feature of CP-FTMW spectrometers has been somewhat underappreciated when the technique is compared to cavity FTMW spectrometers. Structure determinations require the assignment of the isotopologues and in either isotope spiking (like the $H_2{}^{18}O$ water cluster measurements) or natural abundance measurements there will be a large number of weak 'isotopic satellite' transitions that, inevitably, are close to strong transitions from the parent species. In this case, the key performance metric is the frequency resolution at baseline. It has been pointed out that cavity FTMW spectrometers have higher frequency resolution, but this assessment is based on the more common full width at half maximum definition of the resolution. The FID decay in a pulsed jet FTMW spectrometer comes from inhomogeneous broadening due to residual Doppler effects. In a cavity spectrometer where the excitation bandwidth is narrower than the inhomogeneous frequency broadening, there is no way to modify the line shape (although there will be filtering from the high-Q cavity resonator) and strong transitions will give signals at a

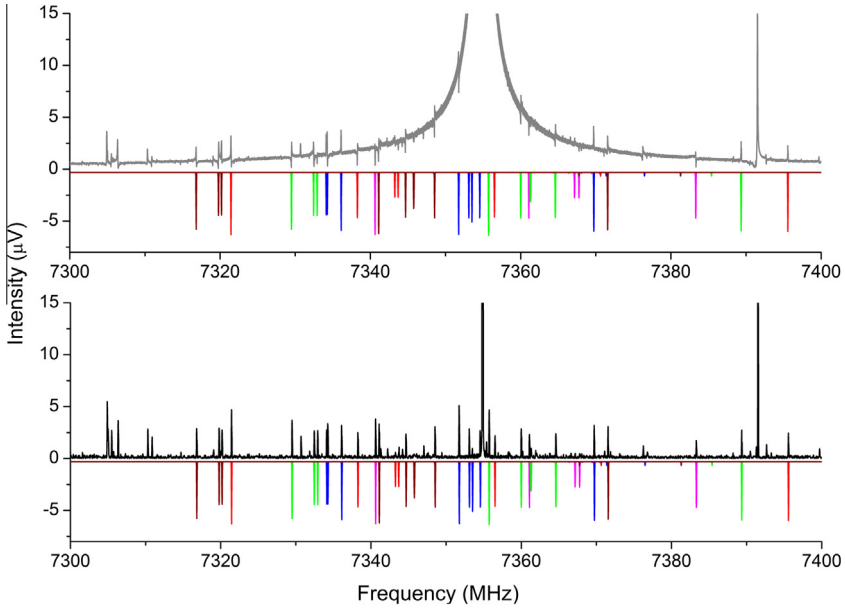

Figure 12. The top panel highlights a portion of the 2–8 GHz spectrum of water after a Fourier transform without applying a window function. The colored traces are 1.5 K (rotational temperature) simulations of the $H_2{}^{18}O$ singly-substituted isotopologues of the water heptamer. The bottom panel covers the same frequency range but after application of a Kaiser-Bessel window to increase the baseline resolution. The intense water dimer line (1_0 B2+ ← 0_0 B2−) at 7354.86 MHz in the middle of the panels obscures transitions belonging to isotopologues when the window function is not applied.

significant frequency offset from the excitation frequency (in the 'tails' of the line shape) and these can obscure weaker transitions in the spectrum. The impulse nature of the broadband CP-FTMW measurement makes it possible to shape the FID envelope using spectral window functions that significantly improve the baseline resolution making it possible to use the full dynamic range of the spectrometer to identify low abundance (or low polarity) species in the presence of species that generate strong rotational transitions. This effect is shown in Figure 12 for a region of the 2–8 GHz spectrum of water.

The analysis of a broadband rotational spectrum of a complex gas sample, like the water expansion that creates wide range of water clusters, poses new challenges to the data analysis. The goal is to assign all spectra in the measurement and then to attribute them to molecular structures (through comparison to predictions from computational chemistry, for example). A strength of molecular rotational spectroscopy is that the Hamiltonian is known for the most common case of an asymmetric rotor with centrifugal distortion. This model can reproduce most rotational spectra to experimental accuracy. Hamiltonians that include other relatively common effects, like internal rotational and nuclear quadrupole hyperfine structure, have been developed by the rotational spectroscopy community. The availability of a quantitative Hamiltonian model makes it possible implement automated searches for the experimental data set for a spectrum consistent with a proposed structure and this greatly speeds the analysis of water cluster spectra, especially for identifying the isotopologue spectra. More sophisticated data mining tools are needed. As an example, the 2–8 GHz spectrum of water used in the heptamer analysis has about 2800 rotational transitions with a signal-to-noise ratio greater than 3:1. So far, we have identified the rotational spectra of 24 water clusters in the size range of 6–15 (3 hexamers, 2 heptamers, 5 nonamers, 4 decamers, 7 undecamers, 2 tridecamers, and 1 pentadecamer). These 24 species only account for about 700 of the observed rotational transitions in the spectrum. As the laboratory data rates increase through the use of high-throughput broadband rotational spectrometers, the field would benefit from the development of an improved, better integrated set of data analysis tools and also of procedures to archive the measured spectra for data mining by the broader scientific community.

3. Conclusions

Advances in high-speed digital electronics have ushered in the era of broadband molecular rotational spectroscopy. These spectrometers provide qualitatively new levels of measurement sensitivity and are expanding the size range of molecules for structure determination. Several groups are advancing broadband rotational spectroscopy methods. Recent work has described spectrometers for pulsed jet microwave spectroscopy in the 2–40 GHz frequency range and the extension to mm-wave spectroscopy for applications to chemical dynamics. Novel molecular beam sources, including pulsed laser ablation, have been incorporated into broadband rotational spectrometers to study fragile biomolecules and to produce novel species like metal containing clusters. Both microwave and mm-wave techniques have been developed for studies of room-temperature gases and these studies are pushing towards real-time, broadband spectral acquisition. New experimental capabilities, like 2D-CP-FTMW spectroscopy, and advanced analysis routines have also recently been described. Some of these techniques are being used in the analysis of interstellar rotational spectra where the new observatories like the Jansky Very Large Array and the Atacama Large Millimeter/Submillimeter Array are now capable of producing spatially-resolved, broadband interstellar rotational spectra for astrochemistry at data rates near 1 TB/day. The technology advances in laboratory and observatory have opened new applications for rotational spectroscopy and moved the field into a new area of big data science.

Acknowledgements

This work was supported by US National Science Foundation (NSF) grants CHE-0960074 and CHE-0848827; grant from the Polish National Science Centre, decision number DEC/2011/02/A/ST2/00298; and NSF grants CHE 0116435, CHE-0521063, and CHE-

0849677 as part of the MERCURY high-performance computer consortium (www.mercuryconsortium.org). This research used the NSF TeraGrid resources provided by the Texas Advanced Computing Center (TACC) under grant TG CHE090095 and resources of the National Energy Research Scientific Computing Center, which is supported by the Office of Science of the U.S. Department of Energy under contract DE-AC02-05CH11231.

S. Lobsiger also thanks Swiss National Science Foundation (grant number 144907).

Appendix A. Supplementary data

Supplementary data associated with this article can be found, in the online version, at http://dx.doi.org/10.1016/j.cplett.2013.04.014.

References

[1] A.L. Steber, B.J. Harris, J.L. Neill, B.H. Pate, J. Mol. Spectrosc. 280 (2012) 3.
[2] G.G. Brown, B.C. Dian, K.O. Douglass, S.M. Geyer, S.T. Shipman, B.H. Pate, Rev. Sci. Instrum. 79 (2008) 053103.
[3] J.K.G. Watson, in: J. Durig (Ed.), Vibrational Spectra and Structure, vol. 6, Elsevier, Amsterdam, 1977.
[4] J. Kraitchman, Am. J. Phys. 21 (1953) 17.
[5] C.C. Costain, Trans. Am. Crystallogr. Assoc. 2 (1966) 157.
[6] W. Gordy, R.L. Cook, Microwave Molecular Spectra, Wiley, New York, 1984. p. 691ff.
[7] J.K.G. Watson, A. Roytburg, W. Ulrich, J. Mol. Spectrosc. 196 (1999) 102.
[8] Z. Kisiel, J. Mol. Spectrosc. 219 (2003) 58.
[9] J.R. Roscioli, D.W. Pratt, Proc. Natl. Acad. Sci. USA 100 (2003) 13752.
[10] P.M. Felker, J. Phys. Chem. 96 (1992) 7844.
[11] B.C. Dian, G.G. Brown, K.O. Douglass, B.H. Pate, Science 320 (2008) 924.
[12] T.J. Balle, E.J. Campbell, M.R. Keenan, W.H. Flygare, J. Chem. Phys. 71 (1979) 2723.
[13] C. Karunatilaka et al., J. Phys. Chem. Lett. 1 (2010) 1547.
[14] M.C. McCarthy, W. Chen, M.J. Travers, P. Thaddeus, Astrophys. J. Suppl. Ser. 129 (2000) 611.
[15] D.P. Zaleski et al., Astrophys. J. 765 (2013) L10.
[16] Y. Ohshima, Y. Endo, Chem. Phys. Lett. 256 (1996) 635.
[17] C. Cabezas et al., J. Mol. Spectrosc. 278 (2012) 31.
[18] J.L. Alonso, C. Pérez, M.E. Sanz, J.C. López, S. Blanco, Phys. Chem. Chem. Phys. 11 (2009) 617.
[19] C. Pérez et al., Science 336 (2012) 897.
[20] S.G. Kukolich, L.C. Sarkozy, Rev. Sci. Instrum. 82 (2011) 094103.
[21] N. Pugliano, R.J. Saykally, Science 257 (1992) 1937.
[22] K. Liu, M.G. Brown, J.D. Cruzan, R.J. Saykally, Science 271 (1996) 62.
[23] K. Liu, M.G. Brown, R.J. Saykally, J. Phys. Chem. A 101 (1997) 8995.
[24] K. Liu et al., Nature 381 (1996) 501.
[25] M.E. Dunn, J. Am. Chem. Soc. 126 (2004) 2647.
[26] A. Lenz, L. Ojamae, J. Chem. Phys. 131 (2009) 134302.
[27] A.N. Tharrington, J. Chem. Phys. A 107 (2003) 7380.
[28] H. Kabrede, R. Hentschke, J. Phys. Chem. B 107 (2003) 3914.
[29] E. Brodskaya, A. Lyubartsev, P.A. Laaksonen, J. Chem. Phys. 116 (2002) 7879.
[30] E. Silva, H.A. Duarte, J.C. Belchior, Chem. Phys. 323 (2006) 553.
[31] H. Takeuchi, J. Chem. Inf. Model. 48 (2008) 2226.
[32] D.J. Wales, H.A. Scheraga, Science 285 (1999) 1368.
[33] J.K. Kazimirski, V. Buch, J. Phys. Chem. A 107 (2003) 9762.
[34] W. Jorgensen, J. Chandrasekhar, J. Madura, R. Impey, M. Klein, J. Chem. Phys. 79 (1983) 926.
[35] D.A. Case et al., AMBER 9, University of California, San Francisco, 2006.
[36] R.M. Shields, B. Temelso, K.A. Archer, T.E. Morrell, G.C. Shields, J. Phys. Chem. A 114 (2010) 11725.
[37] B. Temelso, K.A. Archer, G.C. Shields, J. Phys. Chem. A 115 (2011) 12034.
[38] C. Møller, M.S. Plesset, Phys. Rev. 46 (1934) 618.
[39] F. Neese, Wiley Interdiscip. Rev. Comput. Mol. Sci. 2 (2012) 73.
[40] S.S. Xantheas, C.J. Burnham, R.J. Harrison, J. Chem. Phys. 116 (2002) 1493.
[41] S.S. Xantheas, E. Apra, J. Chem. Phys. 120 (2004) 823.
[42] G.S. Fanourgakis, E. Apra, S.S. Xantheas, J. Chem. Phys. 121 (2004) 2655.
[43] S. Bulusu, S. Yoo, E. Apra, S. Xantheas, X.C. Zeng, J. Phys. Chem. A 110 (2006) 11781.
[44] S. Yoo, E. Apra, X.C. Zeng, S.S. Xantheas, J. Phys. Chem. Lett. 1 (2010) 3122.
[45] T. Dunning, J. Chem. Phys. 90 (1989) 1007.
[46] R. Kendall, T. Dunning, R. Harrison, J. Chem. Phys. 96 (1992) 6796.
[47] S.S. Xantheas, Philos. Magn. B-Phys. Condens. Matter Stat. Mech. Electron. Opt. Magn. Prop. 73 (1996) 107.
[48] W. Klopper, J. Chem. Phys. 102 (1995) 6168.
[49] J.L. Neill et al., J. Mol. Spectrosc. 269 (2011) 21.
[50] AUTOFIT program, available from <http://faculty.virginia.edu/bpate-lab/usefulstuff.html/>.
[51] D. Plusquellic, JB95 package, available from <http://www.nist.gov/pml/div686/sources_detectors/jb95.cfm>.
[52] Z. Kisiel et al., J. Mol. Spectrosc. 233 (2005) 231.
[53] Z. Kisiel et al., J. Mol. Spectrosc. 280 (2012) 134.
[54] H.M. Pickett, J. Mol. Spectrosc. 148 (1991) 371.
[55] H.M Pickett, SPFIT/SPCAT Package, available at <http://spec.jpl.nasa.gov./>.
[56] Z. Kisiel, in: J. Demaison et al. (Eds.), Spectroscopy from Space, Kluwer, Dordrecht, 2001, p. 91.
[57] Z. Kisiel, PROSPE – Programs for ROtational SPEctroscopy, <http://info.ifpan.edu.pl/~kisiel/prospe.htm./>.
[58] E.F. Pettersen et al., J. Comput. Chem. 13 (2004) 1605.
[59] C.J. Gruenloh et al., Science 276 (1997) 1678.
[60] Y. Wang, J.M. Bowman, J. Phys. Chem. Lett. 4 (2013) 1104.
[61] J.O. Richardson et al., J. Phys. Chem. A, Article ASAP (2013), http://dx.doi.org/10.1021/jp311306a.
[62] J. Brudermann et al., J. Chem. Phys. 110 (1999) 10649.
[63] W. Lin, J. Han, L.K. Takahashi, J.G. Loeser, R.J. Saykally, J. Phys. Chem. A 110 (2006) 8011.
[64] M. Losada, S. Leutwyler, J. Chem. Phys. 119 (2003) 304.
[65] F.N. Keutsch, R.J. Saykally, Proc. Natl. Acad. Sci. USA 98 (2001) 10533.

Cristóbal Pérez received his B.S. in Chemistry and his Ph.D in Physical Chemistry from Universidad de Valladolid (Spain) in 2011. His thesis work was focused on the study of biomolecules using laser ablation techniques coupled with rotational spectroscopy. He joined the group of Prof. Brooks Pate in the University of Virginia as a Postdoctoral Research Associate in 2011, where he is currently working. His research interests have focused on the structural characterization of molecules of biological interest as well as hydrogen-bonded complexes, with a special emphasis in the study of water clusters by broadband rotational spectroscopy.

Simon Lobsiger received his Ph.D. and M.S. degrees in chemistry and molecular sciences in 2012 and 2008, respectively, from the University of Bern, Switzerland. He has a B.S. degree in chemical engineering from the Bern University of Applied Sciences in Burgdorf, Switzerland. He is currently working in the group of Prof. Brooks H. Pate at the University of Virginia with a postoctoral fellowship from the Swiss National Science Foundation.

Nathan Seifert received his B.A. degree in Chemistry from Amherst College in Amherst, MA in 2010 and is currently working towards a Ph.D. degree from University of Virginia in the Pate group. His research interests include the spectroscopy and structures of gas phase molecular clusters and scientific computing.

Daniel Zaleski received his B.S. in chemistry from Syracuse University in 2008. He will be completing his Ph.D. in chemistry at the University of Virginia in 2013. Since joining the Pate lab at UVa his interests have focused around astrochemistry and molecular structure of van der Waals clusters. Upon graduation, he has accepted a postdoctoral research position at Newcastle University with Dr. Nick Walker.

Berhane Temelso is a computational chemistry postdoc working with George C. Shields at Bucknell University. He received his Ph.D. in chemistry from Georgia Institute of Technology in Atlanta, GA and B.A. in physics from Berea College in Berea, KY. His research is mainly focused on the application of efficient computational methods to understand the structure and dynamics of hydrogen-bonded systems ranging from water clusters and atmospheric aerosols to biological molecules. His Ph.D. work explored the ability of the most rigorous first-principles computational methods to reproduce molecular properties derived from experiment.

George C. Shields is the Dean of the College of Arts & Sciences and Professor of Chemistry at Bucknell University. He earned B.S., M.S., and Ph.D. degrees at Georgia Tech. He was a postdoctoral associate at Yale University working with Thomas Steitz, where he helped solve the structure of the CAP/DNA complex. He was a faculty member at Lake Forest and Hamilton Colleges, and has developed initiatives to increase the amount of undergraduate research in computational chemistry nationwide. He has worked with more than 100 undergraduates, and almost 90% of his alumni have attended graduate or professional schools.

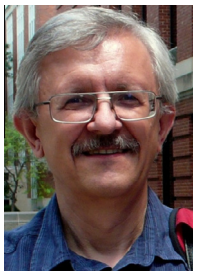

Zbigniew Kisiel received his B.Sc. in Chemistry in 1976, and Ph.D. in Physical Chemistry in 1980, both at the Department of Chemistry, University College London. He joined the Institute of Physics of the Polish Academy of Sciences in 1980, where he is now a Professor of Physics. His Ph.D. work carried out in the Millen group on the $H_2O\cdots HF$ cluster defined several recurrent themes in his later research: applications of rotational spectroscopy to molecular physics (now inclusive of the THz region and astrophysics), properties of weakly bound intermolecular clusters, and the use of computer techniques in rotational spectroscopy.

Brooks H. Pate is a graduate of the University of Virginia and received his Ph.D. from Princeton University (1992). Following a NRC Postdoctoral Fellowship at NIST he returned to the University of Virginia where he is William R. Kenan, Jr. Professor of Chemistry. His group has pioneered the Chirped Pulse Fourier Transform Microwave technique and developed the field of dynamic rotational spectroscopy. He is a fellow of the American Physical Society and the recipient of several awards including a MacArthur Fellowship (2001), the Bomem-Michelson Award (2013), and the Earle K. Plyler Prize for Molecular Spectroscopy and Dynamics (2013).